FLOOR-FRACTURED LUNAR CRATERS

PETER H. SCHULTZ

*NASA Ames Research Center, Space Science Division, Moffett Field, California, U.S.A.**

(Received 6 January, 1976)

Abstract. Numerous lunar craters (206 examples, mean diameter = 40km) contain pronounced floor rilles (fractures) and evidence for volcanic processes. Seven morphologic classes have been defined according to floor depth and the appearance of the floor, wall, and rim zones. Such craters containing central peaks exhibit peak heights (approximately 1km) comparable to those within well-preserved impact craters but exhibit smaller rim-peak elevation differences (generally 0–1.5km) than those (2.4km) within impact craters. In addition, the morphology, spatial distribution, and floor elevation data reveal a probable genetic association with the maria and suggest that a large number of floor-fractured craters represent pre-mare impact craters whose floors have been lifted tectonically and modified volcanically during the epochs of mare flooding. Floor uplift is envisioned as floating on an intruded sill, and estimates of the buoyed floor thickness are consistent with the inferred depth of brecciation beneath impact craters, a zone interpreted as a trap for the intruding magma. The derived model of crater modification accounts for (1) the large differences in affected crater size and age; (2) the small peak-rim elevation differences; (3) remnant central peaks within mare-flooded craters and ringed plains; (4) ridged and flat-topped rim profiles of heavily modified craters and ringed plains; and (5) the absence of positive gravity anomalies in most floor-fractured craters and some large mare-filled craters. One of the seven morphologic classes, however, displays a significantly smaller mean size, larger distances from the maria, and distinctive morphology relative to the other six classes. The distinctive morphology is attributed, in part, to the relatively small size of the affected crater, but certain members of this class represent a style of volcanism unrelated to the maria – perhaps triggered by the last major basin-forming impacts.

1. Introduction

Numerous lunar craters exhibit extensive fracture systems on their floors. Masursky (1964), Daneš (1965) and Pike (1968) suggested that isostatic rebound might account for the fractures and crater profile. DeHon (1971) interpreted two examples, Ritter and Sabine, as resurgent cauldrons. Cameron and Padgett (1974) and Whitford-Stark (1974) generalized the interpretation of an endogenic origin to all floor-rilled craters. Schultz (1972, 1974, 1976), Young (1972), Wood (1974), and Brennan (1975) suggested that many floor-fractured craters represent volcanically modified impact craters.

The present study presents the morphology and interpretation of floor-fractured craters on the lunar near and far sides. The observational data for such craters will be examined first, including their classification, distribution (spatial and size), and floor, peak, and rim elevations relative to the maria. These data contribute to a reconstructed history of crater modification, which is illustrated by two selected examples. Lastly, the significance of floor-fractured craters is considered.

2. Classification and Distribution

Craters can be described by the characteristic morphologies of the floor, wall, and rim zones. This zonal approach permits comparison of different craters without assigning a crater type, which is a result of the different premutations of these zones,

* Current address: University of Santa Clara/NASA Ames Research Center, Space Science Division, Moffett Field, California, U.S.A., 94035.

The Moon **15** (1976) 241–273.

and thus preserves an important distinction between crater *origin* and crater *modification.* Floor-fractured craters represent a floor type that is based on the presence of a single parameter, large floor rilles, and that is associated with wall and rim zones of widely different morphologies. Three parameters can be used in describing such crater floors: fracture pattern; floor depth; floor type. Floor fractures generally do not extend beyond the wall/rim boundary and occur in concentric, radial, and polygonal patterns. Additionally, a characteristic form of concentric fractures occurs as a boundary between the floor and wall, a configuration that produces a moatlike apearance.

The second parameter, floor depth, is largely independent of fracture pattern. As will be discussed below, floor depths range from very shallow (above adjacent units outside the crater) to deep (comparable to the depth of Copernicus).

The third parameter, floor type, is more qualitative. If the formation or development of the crater floor unit is independent of a period of floor fracturing, then it is clear that a wide variety of floor types with fracturing can, and does, occur. The following descriptions of floor types combine the three parameters.

Class I (fractured-floor impact craters) resembles Copernicus in its overall morphology: deep floor, central peak complex, extensive wall slumps, and well-preserved hummocky ejecta blanket (Figure 1a). However, concentric, radial, and/or polygonal fracture patterns cross the floor, and dark mantle deposits commonly surround elongate pits which occur along fractures near the floor-wall boundary. Emplacement of marelike units, which occur in a few examples, postdates the period of floor fracturing. The central peak complex is typically a system of annular peaks, a crescent-shaped peak, or central peak with a summit pit. Although these craters typically are near the shallow maria, two examples (Compton; unnamed near +73°, 165°E) occur deep in the lunar highlands. Where a stratigraphic relation to the maria exists, crater formation predates at least the last stages of local mare emplacement. Examples include Atlas, Einstein A, Schlüter, Cardanus, Petavius, Humboldt, and Lavoisier E.

Class II (shallow, fractured hummocky floor) is characterized by a shallow, hummocky floor bounded by abrupt wall scarps (Figure 1b). The hummocky floor is comprised, in part, of old wall slumps, and interior to this debris in several examples is a polygonally fractured plains region surrounded by concentric fractures. As in Class I, central peaks occur, but less frequently, and five exhibit central depressions. In contrast to Class I, dark-haloed craters and mantling deposits are uncommon. A full range of rim morphologies is displayed; from hummocky Copernicus-like ejecta facies to diffuse or nonexistent blankets. Where a preserved ejecta blanket exists, the rim may be raised. Severed, or 'perched', craters, commonly occur along the scalloped rim. Craters with this morphology occur immediately adjacent to or within the mare plains and predate mare emplacement. Examples are Encke, Davy, Briggs, and Vitello.

Fig. 1. Examples of classes of floor-fractured craters as described in the text. Class I: Atlas (LO IV-74-H2, H3); diameter, 85 km. Class II: Encke (LO IV-138-H1); diameter, 28 km. Class III: Gassendi (LO IV-143-H2); diameter 110 km. Class IV A: unnamed (LO I-115-H1, H2); diameter, 28 km. Class IV B: Gaudibert (LO IV-72-H3, H2); diameter, 36 km. Class V: Repsold (LO IV-189-H3); diameter, 110 km. Class VI: Pitatus (LO IV-119-H3); diameter, 110 km.

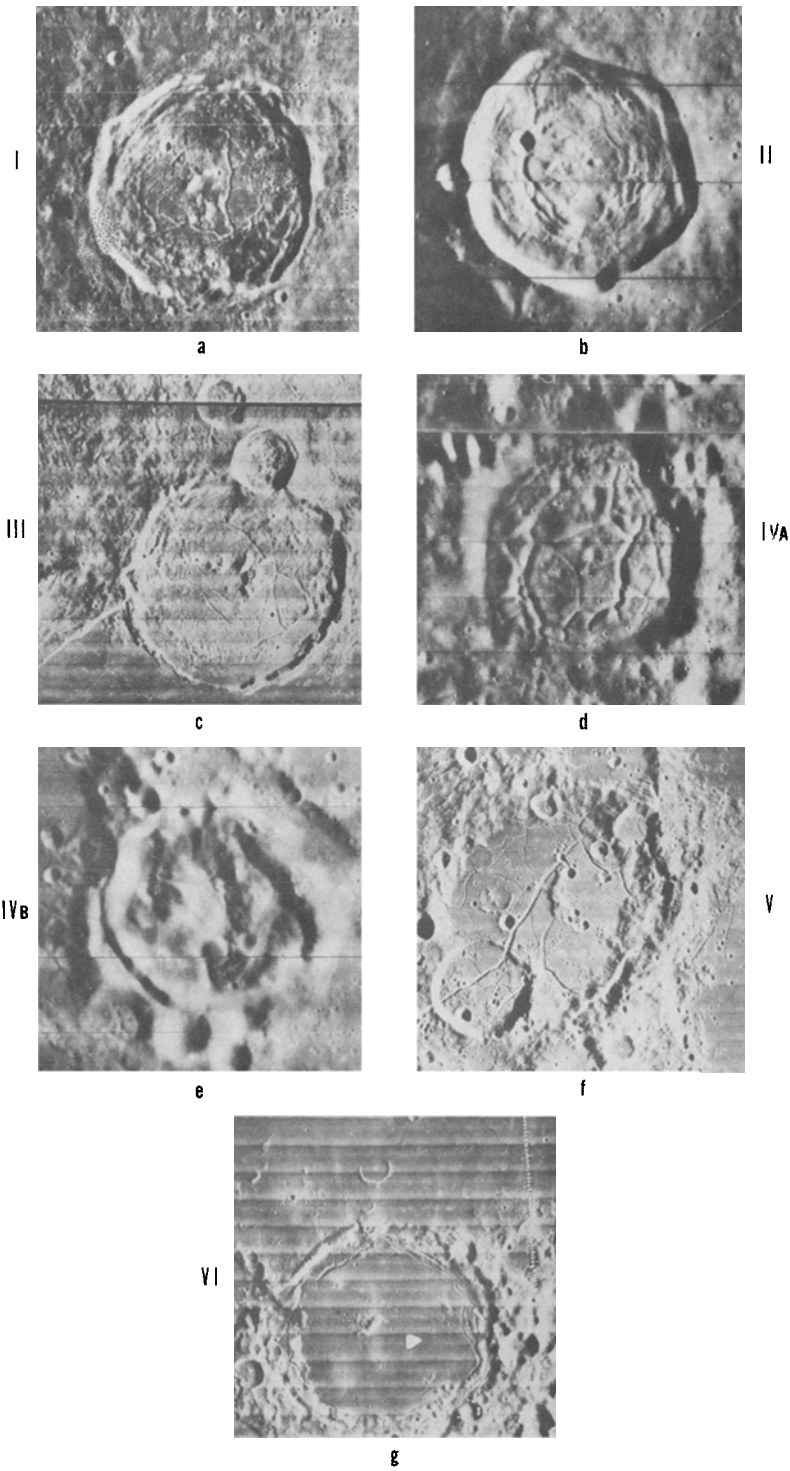
I
a
II
b
III
c
IVA
d
IVB
e
V
f
VI
g

Class III (wide floor moat) craters exhibit a wide annular depression, or 'moat', between a shallow platelike floor and wall scarp (Figure 1c). This moat commonly is discontinuous around the floor and typically is best developed on the side nearest an exterior mare plains. A ridge with a symmetric profile borders the floor plate in several craters, and in the crater Haldane it produces a multi-rimmed crater plan. In other examples, the floor is surrounded by concentric ridges and fractures. The moat may contain marelike or smooth light plains units. The interior floor plate most commonly exhibits polygonal fracture patterns that terminate at the moat. As in the preceding classes, central peak complexes occur and within three craters (Gassendi, Haldane, Posidonius) they are arranged in a semiannular plan. The terrain on the floor plate is generally hummocky but highly subdued and exhibits wide variations in local crater densities. Smooth light plains units also occur on the floor plate and exhibit higher crater densities than do the subdued hummocky terrains. Smooth marelike plains have inundated the inner floor and moat regions of several examples near Mare Smythii, leaving a concentric ring of ridges and hills. Probable volcanic vents (cones and fissures) and low-albedo deposits are common. In the craters Gassendi and Posidonius extensive wall slumps, which are characteristic of large lunar craters, exist on the side farthest from the exterior mare plains. The rim region in Gassendi-like craters may be Copernicus-like or highly subdued. The highly subdued rim facies and profiles are in clear contrast to the wealth of floor detail. Several craters display symmetric ridgelike outer rims, i.e., well-defined slope breaks both interior and exterior to the crater. Where such ridge-like rims occur, an annular depression can be identified exterior to the rim. This type of profile is most typical where the rim is immediately adjacent to the mare plains. Included in Class III are a few shallow craters containing large platforms separated by wide fractures, which are typically filled by mare or light plains units; examples are Gerard Q (inner) and a small craterform south of Airy (6°E, 10°S). Examples more representative of Class III are Gassendi, Posidonius, Doppelmayer, Lavoisier, Haldane, Runge, and Warner.

Class IV (narrow floor moat) craters are similar to the preceding class in that they also are shallow and possess a moatlike feature adjacent to the wall (Figures 1 d,e). However, craters in this class exhibit a much narrower moat that has a V-shaped profile, except where it contains light smooth-surfaced units. The interior border of the moat commonly is ridgelike, and the ridgelike border in Gaudibert is at a higher elevation than the adjacent crater rim on the southwestern side (Class IV B, Figure 1e). Most examples, however, have lower relief ridged borders (IV A, Figure 1d). Interior to the confining moat-ridge, the floor is characteristically subdued and hummocky. It may contain subdued irregular depressions, crater forms, and low-relief acentral knobs. Although well-defined central peaks are generally absent, the three examples (Airy; +16°, 174°E; +17°, 173°E) that possess peaks are similar in overall morphology and peak type: subdued rim and wall, polygonal fracture pattern, highly subdued singular central mound. The floor fractures are highly subdued and are arranged most commonly in polygonal or radial patterns. Concave, convex, and flat floor profiles exist. Wall slumps are generally absent even though the crater may be significantly larger than 15 km, the diameter above which slumping becomes extensive (Quaide *et al.*, 1965; Pike, 1968). Instead, the

wall is a well-defined scarp. A hummocky ejecta blanket also is characteristically absent, but the rim is typically raised, and in a few examples ridgelike. A distinctive feature of this class is the common occurrence as interconnecting doublets or triads. Nevertheless, the floor and encompassing moat typically extend into these adjacent depressions, as well as other minor extensions such as a large wall scallop. Examples of this class are Gaudibert, Bohnenberger, Airy, small craters within Einstein, an example (−16°, 167°E) west of Aitken, and a doublet east of Lavoisier. In general, such craters occur at distances from the maria greater than those for the preceding classes, and numerous examples are found deep in the highlands. A similar class of small (less than 15 km in diameter) contain narrow moats along the wall but fracture patterns on the floor are absent. Floor units include marelike material and light hummocky or plains units. Such craters occur both near the maria and within the highlands.

Class V (fractured light plains) typifies craters that appear relatively unmodified structurally other than the polygonal or concentric arrangement of floor fractures. The floor may be deep or shallow, depending on the state of modification prior to fracturing. The primary floor unit is the Cayley or other light plains material, and a limited eruptive history is indicated by dark-haloed craters along the fractures. The walls generally are hummocky and subdued without well preserved slump blocks, and the smaller examples (less that 25 km in diameter) have subdued furrowed walls. Likewise, the rim region is subdued, both in morphology and profile. Examples include Lavoisier D and Alphonsus. They typically are concentrated near the maria.

Class VI (fractured mare floors) exhibits fractured mare or marelike plains units. Recorded fracture patterns include concentric, polygonal, and radial plans. Pitatus, in particular, contains low-relief central hummocks from which three fractures extend to the major concentric system adjacent to and within the wall region. The prominent concentric fracture system near the wall typifies this class. Although not included in the data below, the crater Tsiolkovsky also exhibits minor concentric fractures in the mare near the wall and radial fractures from the central peak.

Table I and Figures 2 through 4 summarize selected observational data for the different crater classes. Figure 2 shows their size-frequency distributions, and Figure 3 illustrates the distribution for all floor-fractured craters. Figure 4 clearly reveals the clustering of floor-fractured craters near the mare plains or local mare units. These data indicate that Class II and III craters have similar size distributions and comparable percentages of frequency of central peaks. Moreover, they exhibit comparable spatial distributions relative to the mare plains. In contrast to Class II craters, however, Class III craters typically contain dark plains units. Classes I, V, and VI are different in morphology and spatial distribution yet are similar in size distributions. Class IV is distinct from all other classes not only in morphology but also in size distribution (typically smaller sizes) and spatial distribution (farther removed from the maria).

Prominent clusters of floor-fractured craters include those adjacent to western Oceanus Procellarum; around Mare Nectaris; the southern border of Mare Smythii; and a region on the lunar farside encircling the Apollo-Ingenii mare region. Two notable departures from the spatial association between mare and floor-fractured craters also are recognized. First, several major mare-inundated regions are relatively

TABLE I

Class	Example	Number	%	Mean diameter (km)	Central peaks % of Class	Dark plains in % of Class	Mean distance to maria A[b]	Mean distance to maria B[c]	Fracture pattern[d]
I.	Atlas	16	8	101	94	19	240	200	c, p, r
II.	Encke	23	11	31	39	13	180	90	c, p
III.	Gassendi	37	18	37	27	54	20	20	c, p, r, m
IV-A.	Bohnenberger	85	42	23	7	8	300	140	p, nm, (c, r)
IV-B.	Gaudibert	7	3	32	0	0	180	20	p, nm, (c, r)
V.	Repsold	25	12	70	38	16	150	90	p, (c, r)
VI.	Pitatus	13	6	51	15	100*[a]	50	30	c, p, r

[a] by definition

[b] approximate distance to closest major mare plains (area greater than 3×10^4 km^2)

[c] approximate distance to closest mare unit

[d] c = concentric, p = polygonal, r = radial, m = moat, nm = narrow moat; those in parentheses indicate minor occurrence or expression.

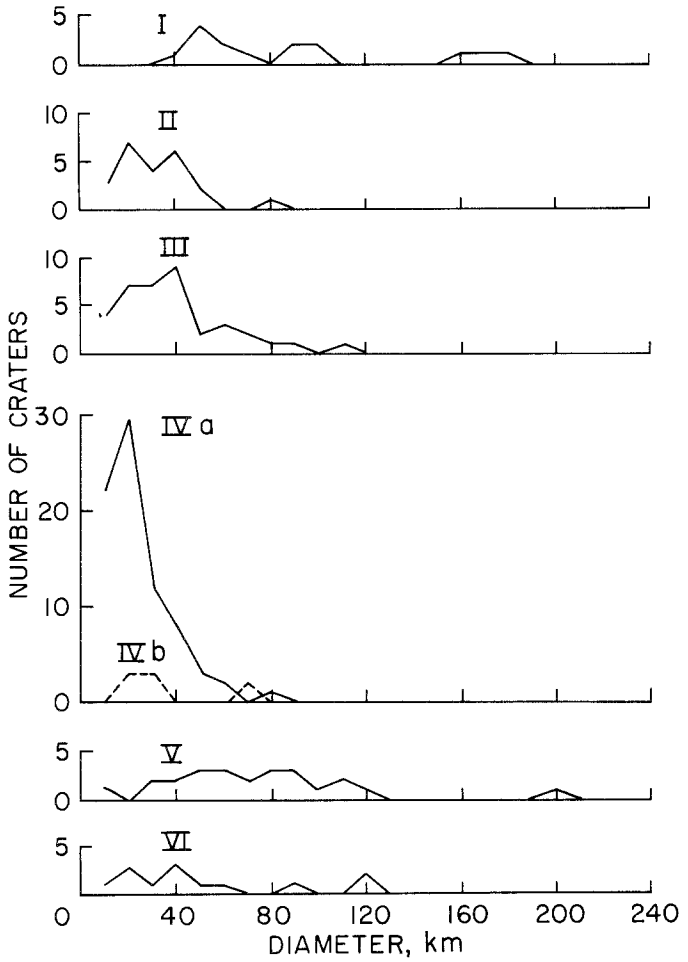

Fig. 2. Histograms for different classes of floor-fractured craters (see Fig. 1 and text).

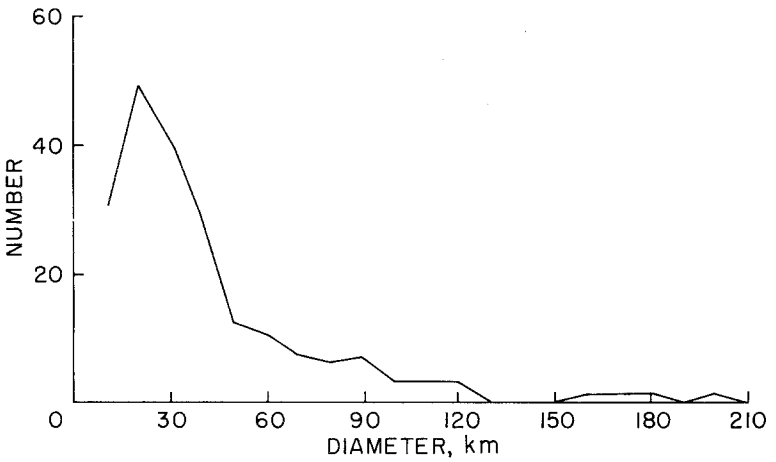

Fig. 3. Histograms for all floor-fractured craters included in this study.

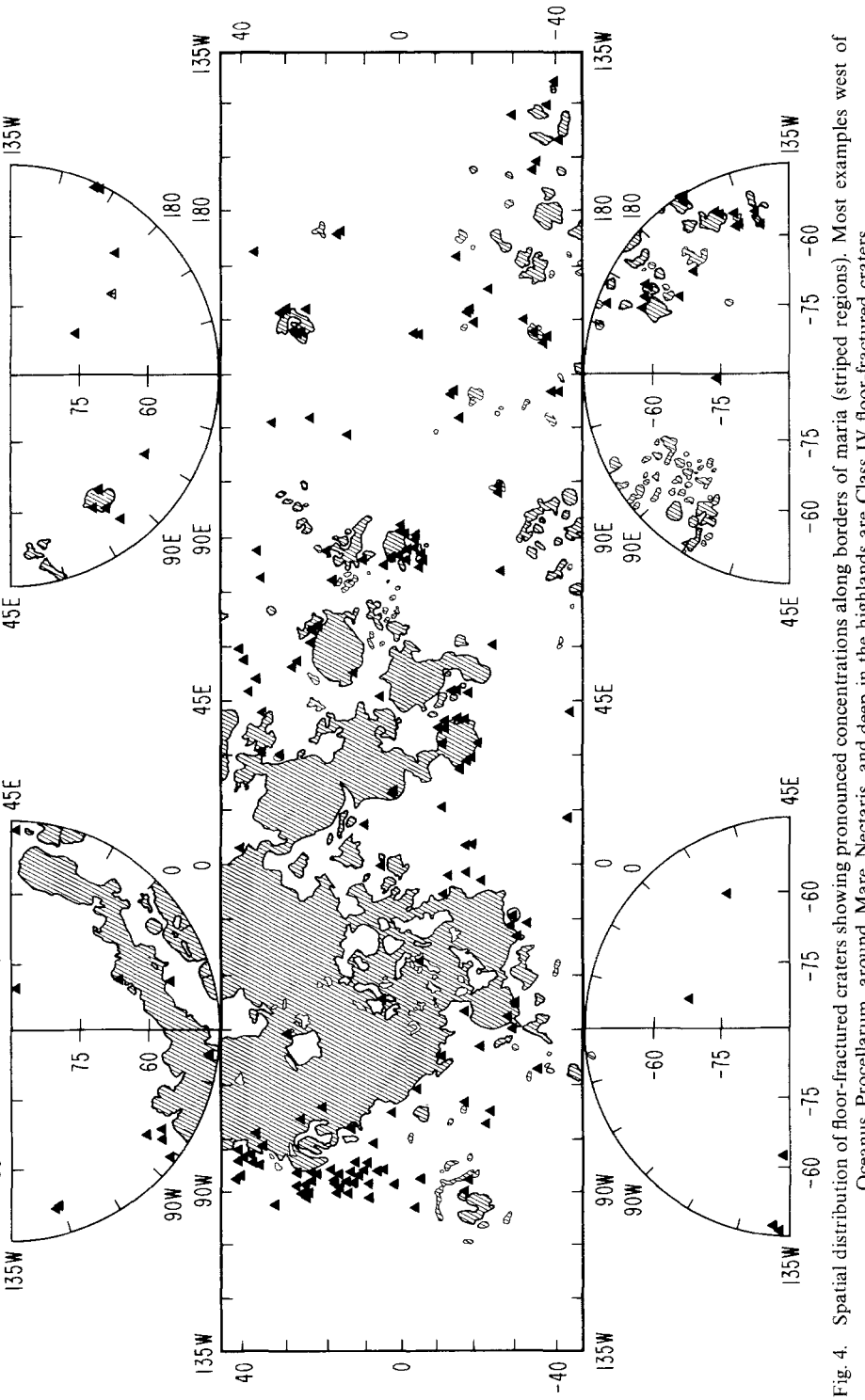

Fig. 4. Spatial distribution of floor-fractured craters showing pronounced concentrations along borders of maria (striped regions). Most examples west of Oceanus Procellarum, around Mare Nectaris, and deep in the highlands are Class IV floor-fractured craters.

devoid of such craters; in particular, Maria Imbrium, Tranquillitatis, Serenitatis, Fecunditatis (eastern), and Australe. Second, a significant number of floor-fractured craters occurs deep in the highland regions.

3. Floor Elevations and Central Peaks

Craters with fractured floors appear to be shallower than fresh impact-produced craters having extensive wall slumps and complex ejecta facies. Figure 5a compares the depths of selected pristine craters (Eratosthenian and Copernican age on the maria) with those of floor-fractured craters. Those values derived from LAC (Lunar Aeronautical Chart) are accurate, at best, to ± 100 m. Rather than adoption of quoted maximum crater depths indicated on the maps, crater depths have been approximated by the difference between the typical elevation of the rim and that of the floor. This approximation eliminates local rim elevation variations due to large scallops or irregular terrain.

Figure 5a contrasts the relatively narrow range of depths for pristine craters to the generally wide range for floor-fractured craters. The pristine-crater depths for a given crater diameter appear to represent an upper limit for fractured-crater depths. Floor-fractured craters in the Mare Smythii region exhibit a narrow range of floor depths (<0.6 km) over a large range of crater diameters. Most of these craters resemble Gassendi or Gaudibert. In general, these two classes and mare-fractured craters are the shallowest, whereas Atlas-like craters are the deepest. The wide range in depths is attributed to craters resembling Encke or Lavoisier D.

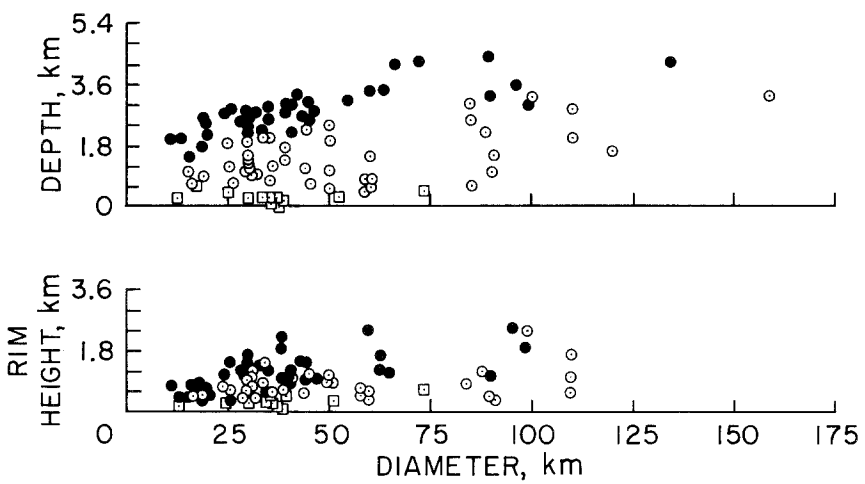

Fig. 5a. (Top). Comparison of typical depths of Eratosthenian and Copernican impact craters on maria (filled circles) with floor-fractured craters (open circles and open squares). Open squares refer to craters near Mare Smythii. Depths correspond to average rim to floor depths and not maximum depths.

Fig. 5b. (Bottom): Comparison of typical rim heights of Eratosthenian and Copernican impact craters with those of floor-fractured craters. Rim heights refer to the typical difference in elevation of the rim from adjacent plains beyond the continuous ejecta blanket. Data represented by circles were derived from LAC maps (accuracy approximately ± 150 m); data represented by squares were derived from LTO maps (accuracy approximately ± 50 m).

Rim height values were also calculated from LAC and LTO (Lunar Topographic Orthophotomaps) contours (Figure 5b) and refer to the elevation difference between the typical rim elevation and the local elevation beyond the bulk ejecta blanket. Most of these data refer to craters within or directly adjacent to the maria where an elevation level can be estimated reliably. In contrast to crater depths, crater rim heights of both floor-fractured and fresh craters are comparable for craters less than 50 km in diameter, but fractured-crater rim heights for diameters greater than 50 km tend to be less than those for fresh impact craters. The latter tendency is also evident for craters in the Mare Smythii region.

If floor elevation is referred to an adjacent (within 100 km) plains unit, then a more striking contrast results between floor-fractured craters and recent impact craters (Figure 6). Whereas the latter class of craters typically has floors 1.5 km beneath the outside terrain, the former class includes floor levels from 1.2 km below to 1.0 km above the adjacent plains. The data for floor-fractured craters near Mare Smythii exhibit a narrower range (from 0.1 km below to 0.4 km above the adjacent plains) than do the remaining data. For comparison, Figure 6 includes relative floor elevations for mare-filled craters. These floors exhibit elevations comparable to the floor-fractured craters. Note that the floor elevation difference for recent impact craters does not appear to increase with crater diameter.

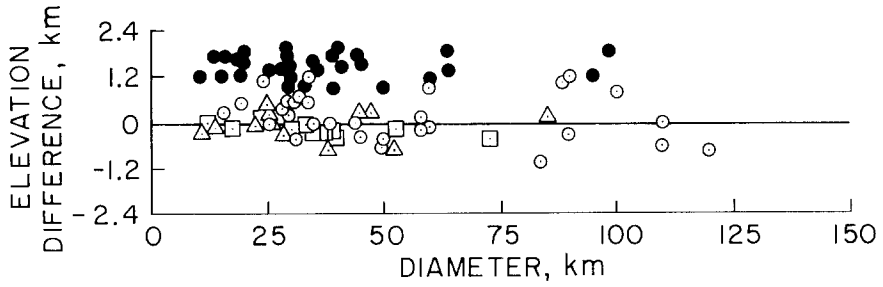

Fig. 6. Typical difference in elevation between plains region outside ejecta blanket and crater floor for: Eratosthenian and Copernican impact craters on the maria (closed circles); floor-fractured craters (open circles and open squares); and mare-filled craters (open triangles). Data for Mare Smythii (open squares) were derived from LTO charts; all other data from LAC maps. Negative elevation difference refers to floor levels above the surrounding plains.

Central peak complexes within impact and floor-fractured craters provide additional data for comparison. Figure 7a shows that central peak heights in both crater types are similar although there is a tendency for peaks in floor-fractured craters to be lower in relief. However, the peak-rim elevation differences for floor-fractured craters (Figure 7b) are significantly smaller than those for well-preserved impact craters. Exceptions to this rule are peaks within slightly modified Atlas-like craters (Class I), which exhibit large (greater than 1.5 km) peak-to-rim elevation differences. Three floor-fractured craters contain central peaks that extend above the rim.

Figure 7b also includes the rim-floor elevation difference (depth) for mare-filled craters without central peaks and the rim-peak elevation difference for mare-filled

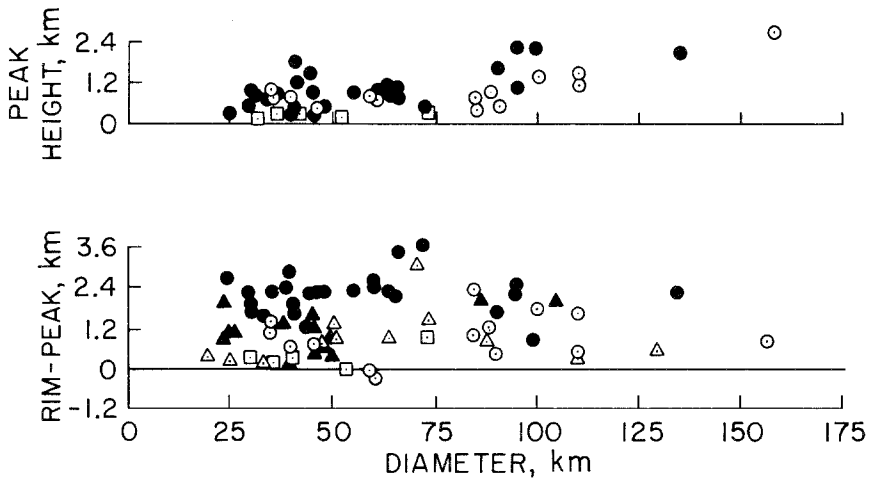

Fig. 7a. (top): Heights of peaks within: Copernican and Eratosthenian impact craters (closed circles); floor-fractured craters (open circles and open squares).

Fig. 7b. (bottom): Difference between typical rim elevation and central peak summit elevation for: Copernican and Eratosthenian impact craters (closed circles); floor-fractured craters (open circles and open squares); mare-filled craters (open triangles). Closed triangles refer to the rim-floor depth of mare-filled craters without central peaks. Data for craters near Mare Smythii were derived from LTO charts; all other data from LAC.

craters containing central peaks. In general, mare-filled craters exhibit depths less than the peak-rim elevation difference for impact craters; thus, mare units may have buried the central peak complex. However, central peaks that remain exposed within mare-filled craters display peak-rim elevation differences significantly below those within pristine impact craters and comparable to those within floor-fractured craters.

Central peaks in several floor-fractured and mare-flooded craters are arranged in annular or crescentic plans. Such plans could be used as evidence for central volcanic structures, but Figure 8 illustrates that this morphology also occurs within unmodified

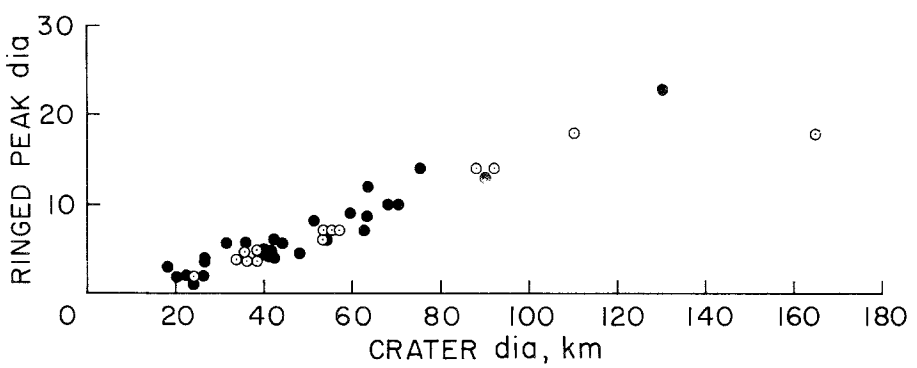

Fig. 8. Comparison of crater diameter and diameter of annularly arranged central peak complexes within unmodified impact craters (closed circles) and floor-fractured craters (open circles) on the lunar nearside.

impact craters of comparable sizes. Within impact craters, the annular arrangement has been interpreted as collapse of the central portion of the uplifted peak complex immediately after crater formation (Baldwin, 1963; Schultz, 1972). The diameter of these central peak rings and pits increases linearly with crater diameter and is distinct in relative size from the central rings within much larger craters and basins. Figure 8 shows that ringed peaks within floor-fractured craters follow the same relationship with crater diameter. Thus both the peak heights and peak morphology within floor-fractured craters are comparable to those within well-preserved impact craters, but the primary difference is the peak-rim elevation difference.

4. Discussion

A. SEQUENCE OF CRATER MODIFICATION

The foregoing morphologic observations and statistical data are summarized in Table I and permit the reconstruction of idealized models of crater modification. Figure 9 provides a reference for the interpreted sequence (Figure 10) from the

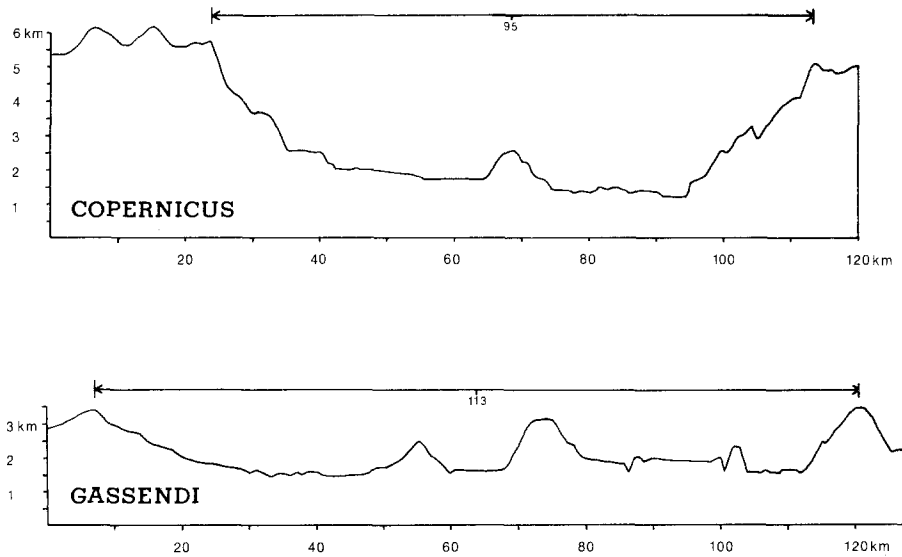

Fig. 9. Comparison between profile of Copernicus (above) and that of Gassendi (below). Vertical exaggeration is a factor of 5. Contours for profiles are from Lunar Topographic Map of Gassendi (sheet B) and Lunar Topographic Map of Copernicus. Both profiles trend NW-SE and pass through the center of the craters.

profile of an unmodified crater (Copernicus) to that of a Class III floor-fractured crater (Gassendi). As will be noted, different stages in this sequence also correspond to other classes of modified craters. Morphologic evidence for the depicted crater history is derived from detailed studies of features associated with floor-fractured craters and is indexed in Table II. Selected features in this sequence as illustrated by the crater Gassendi (Figure 11) are discussed below.

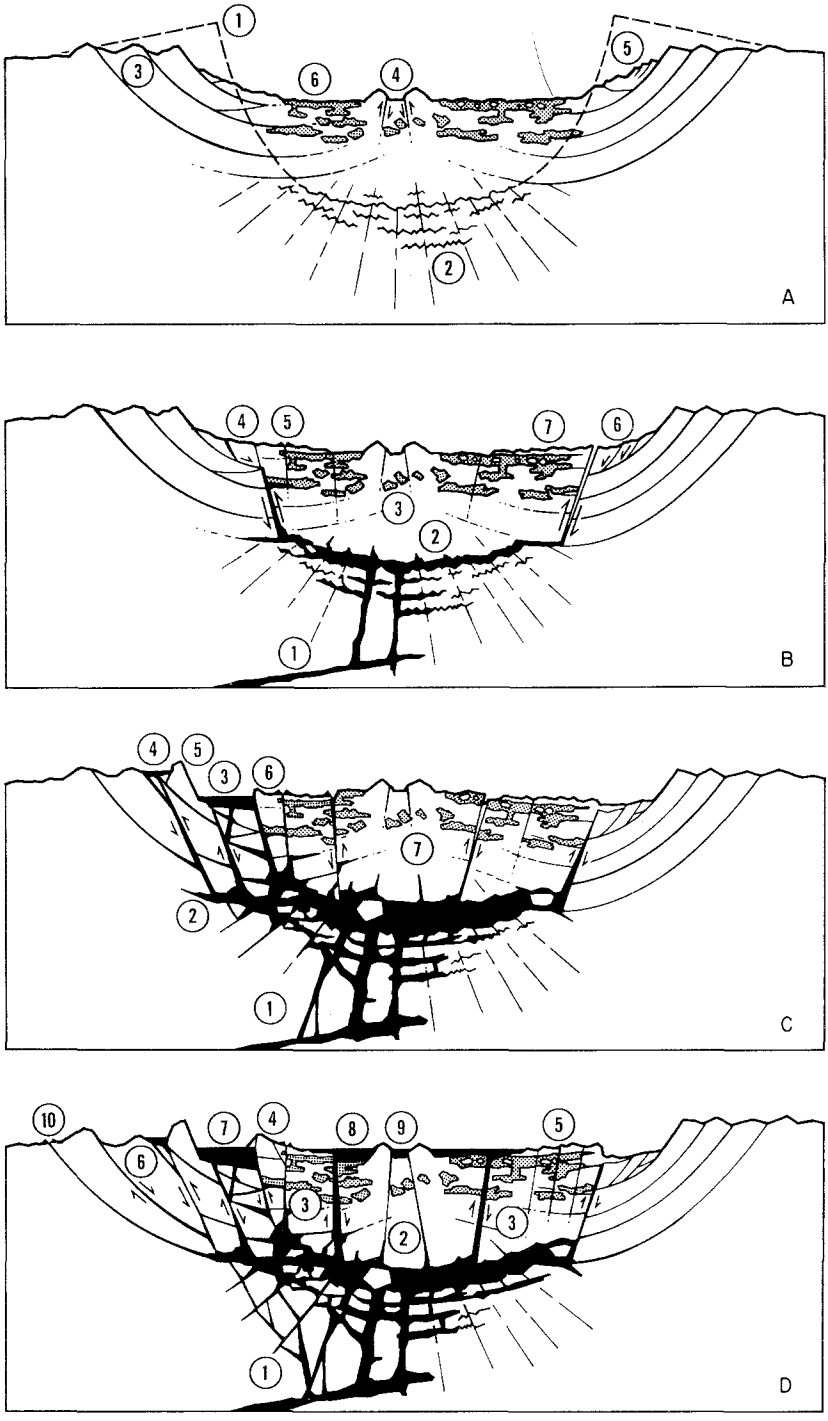

Fig. 10. Idealized sequence in the development of floor-fractured craters (Classes I, II, III). Numbers refer to features discussed in the text and summarized in Table II. Profiles are based on those of Copernicus and Gassendi and represent a vertical exaggeration of a factor of 5. Dashed profile in A indicates the excavation crater profile (prior to rim collapse immediately after formation).

TABLE II

Index to sequence of floor modification depicted in Figure 10

STAGE	REGIONS AND EVENTS OF INTEREST	EVIDENCE, RATIONALE, COMMENTS
A. Initial impact crater	1. Idealized excavation crater	1. From small-scale impacts
	2. Fractured crust beneath crater	2. From estimated shock pressures
	3. Slumps producing annular ridges beyond rim/wall scarp and enlarging excavation crater	3. From crater morphology
	4. Central peak complex with dropped central region	4. Annular and crescentic plan of central peaks in impact craters smaller than 100km
	5. Perched wall slumps	5. Indicated by morphology
	6. Cap of impact melt extruded from trapped pockets of melt and cascades from wall	6. Volcanic cones, fissures, and flow textures on floors of large impact craters
B. Initial structural and volcanic modification (Class I and II)	1. Sill or dike from major magma chamber intersecting fractured zone beneath impact crater	1. Proximity to maria and variety in size and age of affected craters
	2. Formation of sill within region between highly fractured zone and fall-back breccia	2. Crater modification restricted to floor
	3. Floor slightly elevated due to intrusion; floor acts as cohesive block owing to welded melt	3. Minor floor modification other than floor fractures
	4. Floor uplift produces marginal concentric fractures; floor separates beneath wall	4. Topographic data
	5. Minor volcanic eruptions along floor edge where fractures extend the deepest	5. Dark-haloed craters typically along fractures near the floor edge
	6. Landslides triggered by further floor uplift	6. Walls exhibit scarps without terraces
	7. Accumulation of mass-wasted wall debris around floor	7. Subdued hummocky material encircles inner floor; subdued fractures in this material reflect incompetency
C. Floor uplift (Class III)	1. En bloc floor uplift produced by greater volume of intrusion	1. Small elevation difference between rim and central peak summit
	2. Feeder dikes offset toward magma source producing asymmetry in magma reservoir	2. Although entire floor is raised, primary volcanism occurs on side closest to adjacent mare basin
	3. Concentration of mare basalts within structural moat on side nearest maria owing to offset reservoir and regional tilt toward mare basin	3. Based on observation noted in (2)
	4. Eruptions of mare basalts and low-albedo pyroclastics along fissure encircling rim	4. Mare units, dark-haloed craters, spatter cones occur in arcs adjacent to rim in heavily modified and mare-filled craters
	5. Development of flat-topped and ridgelike rim profile owing to encircling graben or rejuvenation of old wall slumps	5. Ridgelike wall/rim of Class III craters with inward and outward-facing scarps
	6. Raised lip on edge of moat attributed to old wall debris perched on uplifted floor edge	6. Annular moat at edge of floor traceable into hummocky wall debris
	7. Separation and uplift of inner floor block including central peak complex	7. Fractures encircle central peak complex with scarp height greater on inner block
D. Partly or completely inundated floor (Class III, V)	1. Network of feeder dikes beneath magma reservoir farther offset toward maria	1. More extensive volcanism indicated on mare side of crater
	2. Floor block divided into several buoyed masses owing to periods of uplift and subsidence; central floor block subsides	2. Extensive fracturing with mare "pool" in central region
	3. Marginal floor region tilted inwards or elevated	3. Suggested by mare inundation of inner floor
	4. Raised rim of moat produced by tilted floor block, remnants of wall debris, and volcanic products	4. Inner ring commonly continuous and symmetrical in profile; ridgelike profile enhanced by emplacement of interior plains
	5. Concentric high-albedo ridges due to fractures in exposed outer floor	5. Merger of ridges with old fractured floor and hummocky wall
	6. Extensive structural modification of rim expressed by annular graben and horst	6. Annular depressions result in concentric rims; original crater rim difficult to identify
	7. Moat region inundated by basalts and represent one of last eruptive sites	7. Marelike plains fill moat; volcanic cones and other possible vent structures occur
	8. Inner floor block inundated by basalts	8. Smooth low-albedo plains cover inner floor
	9. Central peaks remain exposed through thin cap of floor lava	9. Small rim-peak elevation differences within some mare-filled craters and ghost rings
	10. Pyroclastic eruptions occur along fractures encircling crater	10. Dark-haloed crater complexes occur along rilles encircling crater

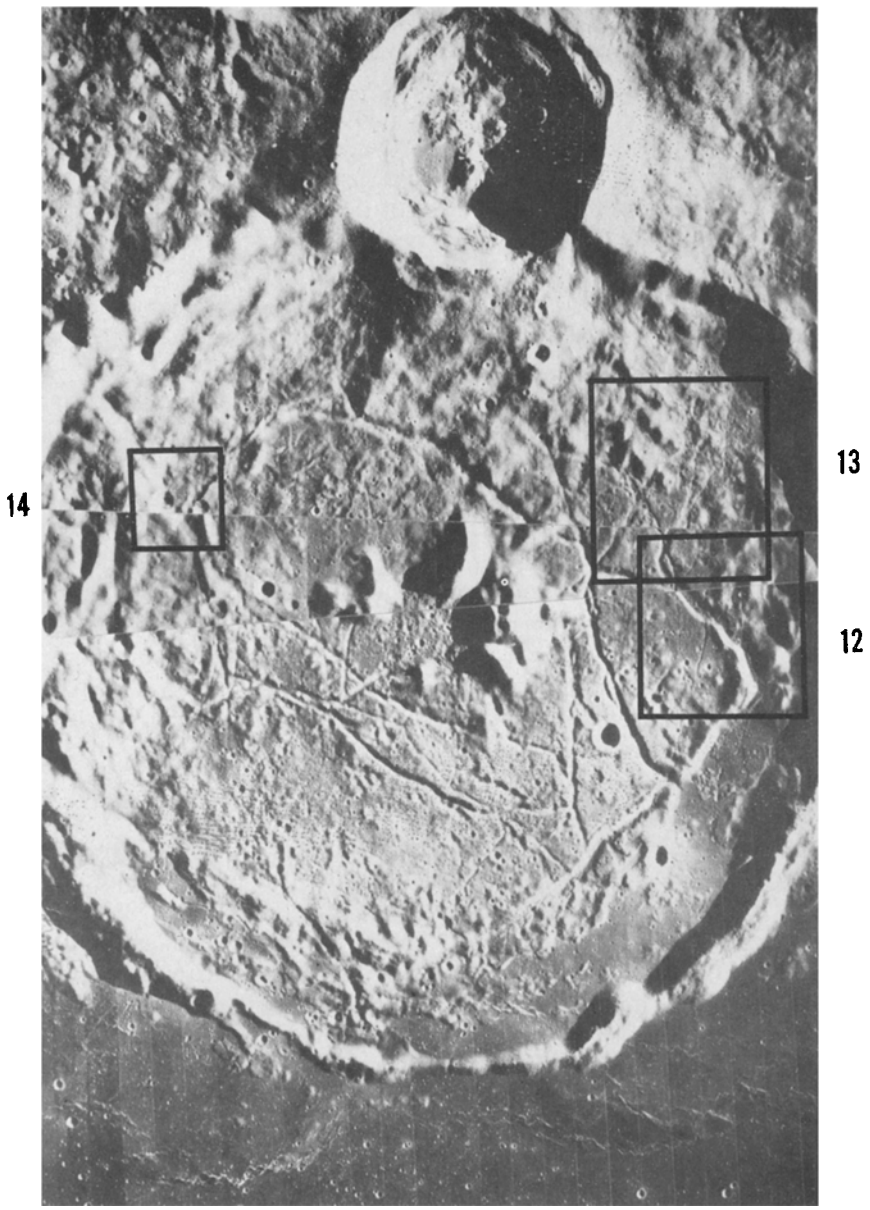

Fig. 11. The Class III crater Gassendi (110 km in diameter) situated on the northern edge of Mare Humorum. Outlined areas correspond to those shown in Figure 12–14. (LO V-177, 178, 179-M).

The initial structure (Figure 10a) corresponds to an unmodified impact crater similar to Copernicus. More typically, the initial crater form is subdued owing to long-term meteoritic erosion or catastrophic modification by major impact basins. The profile (note the vertical exaggeration) indicated by the dashed lines represents the idealized transient crater, i.e., the crater shape at the end of the excavation stage

(see Gault *et al.*, 1968). Beneath the crater the impact extensively fractured the lunar crust concentric and radial to the shock point. Any pre-existing fracture systems probably would have been enlarged during the passage of the intense shock wave. Following the excavation stage, extensive slumping occurs and enlarges the crater as much as 25–40 % (Quaide *et al.*, 1965). Although the most obvious slump remnants are along the crater wall, slumping also extends beyond the abrupt rim-wall transition, which corresponds to the crest of the wall scarp. Massive deep-seated slumping and lateral flow during relaxation from the transient crater form are believed to contribute to the formation of the central peak complex. The central peak complex in this illustration contains a central down-dropped region as interpreted from the annular or crescentic arrangement of massifs illustrated in Figure 8.

Impact melt caps the rubbled floor owing to both local extrusions within the floor rubble and cascades of melt from the lower wall region. The total volume of this impact melt is not known. Estimates range from direct and probably unrealistic (Gault, personal communication) extrapolation of small-scale impact data, where most of the melt is ejected, to estimates by Dence (1971) where the melt accounts for most of the floor material.

Modification of the impact crater in Figure 10a is depicted in the subsequent diagrams. Owing to the close spatial association of floor-fractured craters to the mare plains, modification is believed related to the epoch of volcanism responsible for the maria. Tapping of magma may have occurred either immediately after impact (Masursky, personal communication) or at a temporally unrelated stage. Figure 10b illustrates an early stage in the structural modification of the crater floor produced by volcanic intrusions. It is assumed that the feeder for these intrusions is one of several deep-seated fractures that extends indirectly to the mare-related magma chamber and intersects the heavily fractured zone beneath the pre-existing impact crater. The ill-defined contact between the highly fractured zone and the accumulation of floor rubble and fall-back breccia represents a region that traps the intruding magma. The floor and mare elevation data strongly suggest magmastatic equilibrium with the level of the surrounding maria as one possible driving mechanism of this intrusive process. Above the brecciated zone, the floor acts as a relatively cohesive block perhaps due to welding performed by retained impact melt and/or the overall low bulk density of the floor. Consequently, the floor is raised *en masse* although minor tensional fractures are propagated within the block. Separation of the floor block occurs near or beneath the old floor-wall contact and generates concentric fracture patterns along which minor volcanic eruptions occur.

The resulting appearance at this early modification stage may resemble Class I, if the extensive ejecta blanket has been preserved, or Class V if the crater has been previously modified by basin ejecta or other degradational processes. Both classes represent craters that have not undergone appreciable floor uplift, and Class V, in particular, typically does not exhibit blocklike floor movement.

Figure 10b also includes features of more advanced modification in which landslides are triggered as a result of appreciable floor uplift. Debris extends across the floor, and the crater wall becomes a well-defined scarp, distinct from the

typically slumped wall region of unmodified or slightly modified craters larger than 20 km in diameter. This stage is believed to correspond to Class II craters. Fractures in such craters generally will be preserved in the innermost floor where wall debris has not covered them or where surface expressions of well-defined fractures are not readily masked by continual mass movement. It was noted above that the interior floor of several Class II craters exhibits a plains unit unlike those within typical pristine impact craters; consequently, the modification leading to Class II craters may have been accompanied by extrusions of light plains materials, either as lava or ash.

One of the controlling factors of floor elevation is the isostatic adjustment between the intruding mass and the mass directly above it. If the original intrusion was restricted beneath the floor, then the adjustment is approximately governed by the mass difference between the unfilled crater and the surroundings. During floor uplift, landslides transfer rim and wall material to the floor and widen the crater, processes that reduce the mass deficit directly above the intrusion. Such a sequence perhaps accounts for Class II craters where the driving force for floor elevation was lessened and extensive floor volcanism, less likely. If crater floor adjustment already was approximately balanced, then extensive wall slumping may bury previous stages of floor volcanism and halt further floor elevation.

This stage of crater modification is also applicable for other craters not exhibiting floor fractures. Specifically, the diameter of the crater Calippus (31 km) is well above the typical limiting size (15 km) above which extensive wall slumping occurs (Pike, 1968), yet wall slumps are absent. At Lunar Orbiter IV resolution, fractures are not easily identified although Orbiter V photography reveals minor systems. Numerous other craters exhibit such slumpless but scarped (30° slope) walls and flat complex floors (Schultz, 1972), among them are Dawes and Krieger. Within these craters, the fractured or extrusively modified floor typically has been buried by wall debris although there is evidence that limited subsequent extrusions were emplaced, e.g., on the floors of Calippus and Krieger, the latter exhibiting a sinuous rille extending from a narrow breach of its wall.

As the magma reservoir beneath the crater floor enlarges, the floor block rises (Figure 10c). Structural modification extends beyond the crater floor, as defined by the base of wall rubble, but remains restricted to the original 'excavation' crater zone. Consequently, portions of the lower wall are elevated with the floor block and form, in part, the raised rim of the floor edge – an interpretation based on morphologic evidence within Gassendi (Figure 12, arrow A) and Taruntius. Figure 10c also indicates that the feeders to the reservoir may be offset from the crater center toward the adjacent maria. The offset results in a concentration of intrusives beneath the floor closest to the maria (Figure 11) and is believed to be expressed on the surface by inundation of this side of the floor by erupted mare units. Additional asymmetry in mare flooding results from regional subsidence toward the adjacent mare plains. If the floor region represents a floating block, it would remain relatively level whereas the surrounding region would dip toward the plains. In effect, the floor is hinged at the base of the wall away from the maria, and greater mare filling occurs in regions of lowest elevation at the base of the opposite wall.

Fig. 12. Eastern floor of Gassendi (see Fig. 11) exhibiting remnants of wall debris on floor that form a raised rim profile of wide moat (A); possible volcanic cones (B,C); marelike plains unit (D) separated from the mare-filled moat to the south; high-level lava mark within moat-fracture (E). Illumination is from the right (east); framelet width is approximately 4.2 km (LO V-178-M).

Typically, extruded mare units are contained within the moat created by the uplifted floor block. Sources for these mare units are believed to be ring fissures along the old wall slump faults and along marginal fractures produced by floor uplift. The active volcanism and tectonism in this region is illustrated along the northeastern wall of Gassendi (Figures 11 and 13) where a portion of the old wall slumps has been removed and a subsided lava lake now remains as expressed by a terraced depression (Figure 13, arrows A, B) and an insular terraced platform (Figure 13, arrow C). Lava drainage from this region contributed to the lava-filled moat along the southeastern wall of Gassendi. In addition, eruptions of mare basalts occur along the rim through fractures produced by the intruding mass and through pre-existing weaknesses expressed by slump faults extending into the rim region. Such parasitic eruptions are common around extensively fractured craters (Doppelmayer) and mare-filled craters (Puiseux) adjacent to or surrounded by mare plains. The profile of the rim in this region also is structurally modified to a

Fig. 13. Northeastern floor region of Gassendi (see Fig. 11) illustrating: irregular depression bounded by scarp (A, B); insular platform within depression (C); absence of wall slumps (D). Illumination is from the right (east); framelet width is approximately 4.2 km (LO V-178-M).

relatively symmetric ridge or plateau, profiles illustrated by the southeastern rim of Gassendi (Figure 9) and Doppelmayer. In Figure 10c, this modification is represented by uplift of the inner rim and subsidence of the outer rim, but complex synthetic and antithetic faulting also probably contributes to the rim profile.

The stage in Figure 10c corresponds to Class III craters, in which extensive structural modification has taken place. Close examination of Gassendi reveals a complex volcanic history as well. The inferred volcanism is represented not only by the emplacement of mare units but also by the formation of small cones (Figure 12, arrows B and C), nested craters (Figure 14) interpreted as a multiphased eruptive product, possible flow units on the inner floor region, and subsided lava lakes. Moreover, perched marelike units (Figure 12, arrow D) and high-level marks within both floor fractures and the wide moat (Figure 12, arrow E) suggest that inundation of the floor by lava was much greater than what is indicated by the present level of the mare basalts. Thus the sequence of floor modification probably was

Fig. 14. Wall terrace within 3 km diameter crater on western floor of Gassendi (see Fig. 11). Continuous nature of terrace creates a nested-crater appearance, a common feature within floor-fractured craters and near mare borders. This and similar craters are interpreted as remnants of multiphased volcanic eruptions.

multi-phased in which periods of uplift and lava inundation were followed by subsidence and lava drainage.

Further modification results in a partly or completely inundated crater (Figure 10d). The network of fractures beneath the crater fills with magma, and the floor block separates into several buoyed masses. In the schematic profile, the central floor block subsides and the encircling blocks rise. Concentric ridges of low-relief, high-albedo ridges encircling the inner mare-inundated floor of craters, particularly in Mare Smythii, are attributed to concentric fractures in the exposed portions of the peripheral floor block. In addition, craters such as Haldane exhibit a pronounced and relatively continuous raised rim at the edge of the floor plate. This rim is interpreted as the edge of the inward tilted floor block (Figure 10d-4) in contrast to the perched wall remnants indicated at Figure 10c-6. The ridgelike profile is enhanced by the combination of inner floor subsidence and subsequent emplacement of lava plains.

Structural modification of the rim region becomes more extensive and results in a concentric graben-horst encircling the old rim (left side, Figure 10d), which is fully expressed around the crater Haldane in Mare Smythii. The concentric graben-horst arrangement and the inner floor block rim produce a multi-ringed crater plan, and the identification of the original crater rim becomes difficult. The concentric graben-horsts result from either subsidence or concentric inward-dipping fracturing (perhaps analogous to cone sheets) above the enlarged intrusion beneath the crater.

Extrusions of lava largely mask the old crater floor. The most active site typically remains in the moat region at the edge of the floor, but inundation of the inner floor also occurs, leaving only the tops of the old central peak complex. Exterior to the crater, parasitic eruptions of low-albedo pyroclastics are centered along fractures encircling the old crater rim or the graben-horst ring. The crater Kiess near Mare Smythii illustrates this stage in partial completion.

Further inundation by erupted lava results in a ghost crater resembling the Flamsteed Ring, Sinus Iridum, and Letronne. Moreover, the ghost ring Lamont is interpreted as a still later stage of inundation where the impact crater was completely inundated.

Several qualifications should be made in this idealized sequence. First, it is obvious that not all floor-fractured craters evolve to the last stage (Figure 10d), and filling of the floor by mare basalts could occur at any stage. For example, the crater Schlüter has been partly inundated with only minor floor elevation. However, the small peak-rim elevation differences of many mare-filled craters (Figure 7b) suggest that considerable floor elevation occurred prior to inundation. Second, the parasitic rim eruptions have been depicted as relatively minor, but these sites may have been important contributors to local inundation. For examples, low-albedo mare units surround the mare-side rim/wall of Gassendi and Doppelmayer. In addition, the mare-filled craters Marius, Plato, and Prinz all have the heads pits of sinuous rilles on their rims. Third, the sequence in Figure 10 illustrates an asymmetric modification and inundation sequence. This permits elaboration on the source of the magma reservoir, but such an arrangement is not typical of floor-fractured craters farther from the mare shore. Fourth, the sequence is based on observations of the end result of several different craters, and there is evidence that such floor-fractured craters have undergone a complex series of uplift and subsidence.

Class IV floor-fractured craters depart from the sequence described in Figure 10. Whereas the other classes of craters exhibit evidence for an intial appearance resembling an impact crater, this class typically lacks such similarities – an expression of extensive modification or a different origin entirely, i.e., caldera collapse. Figure 15 illustrates an alternate sequence in development (indexed in Table III) and Figure 16 illustrates pertinent features. The first stage (Figure 15a) is represented as a craterform (impact crater or caldera) that already has been modified by intrusions. The relatively shallow floor and interior light plains suggest that floor elevation is perhaps due to both floor uplift and extrusions of light-colored ash and lava. The relatively high albedo of these extrusions might indicate assimilation of highland material into the intruding magma.

Whereas uplift in Class III craters affects the central floor region separated from the outer wall scarps, Class IV craters (by definition) exhibit uplifted floors

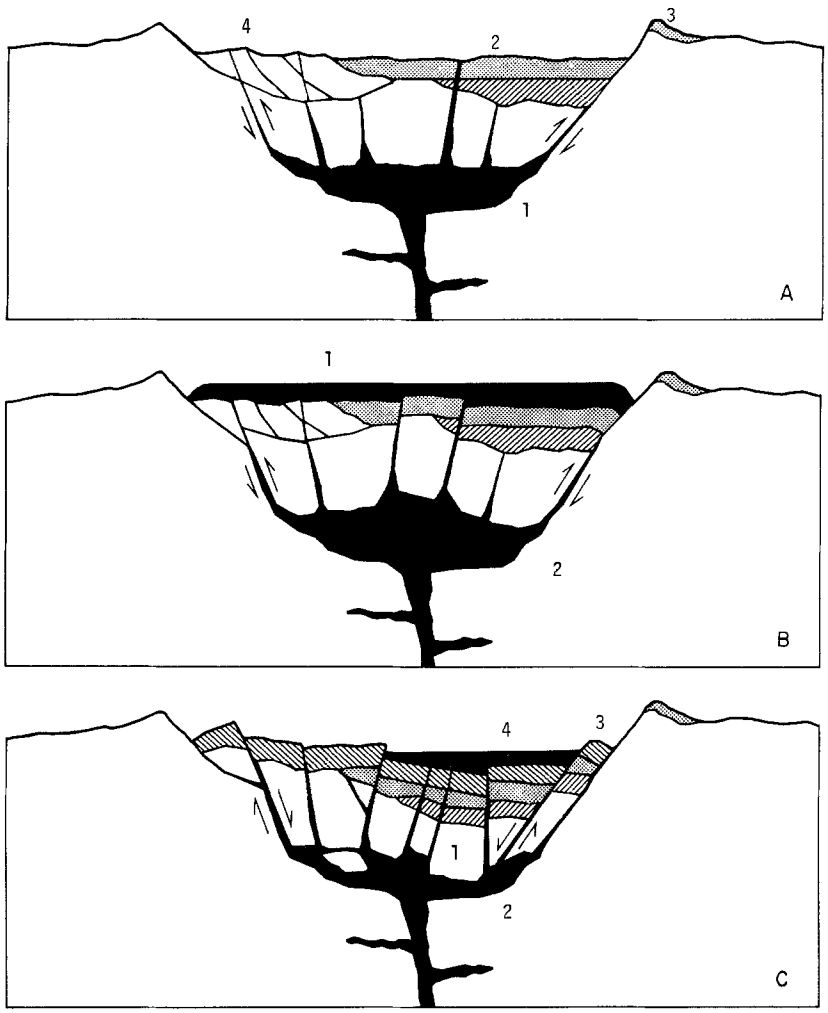

Fig. 15. Idealized sequence in the development of Class IV floor-fractured craters. Numbers refer to discussion in Table III and the text.

extending to the wall scarp. This might be a result of crater size as well as floor-filling eruptions. Figure 2 and Table I show that most Class IV craters are significantly smaller (mean diameter 22 km) than all other floor-fractured crater classes. This is the size range in which slumping becomes an important modifier of crater diameter (Quaide *et al.*, 1965; Pike, 1968). Impact craters above this size range may be enlarged by as much as 40%; thus their present diameter does not reflect the transient crater diameter. Impact craters smaller than this size range, however, will resemble more closely the transient crater diameter. Consequently, modification of the floor region will extend to the crater wall although later slumping triggered by floor movement probably does increase the diameter slightly.

Figure 15b illustrates a stage represented by numerous Class IV A craters. Extrusions of light-colored flows or ash have resulted in an entirely new floor surface

TABLE III

Index to sequence of floor modification depicted in Figure 15

STAGE	REGIONS AND EVENTS OF INTEREST	EVIDENCE, RATIONALE, COMMENTS
A. Modified crater	1. Magma reservoir beneath craterform responsible, in part, for floor uplift	1. Shallow depth of crater due to crater fill and/or floor uplift
	2. Extrusions of light-colored ash and lava also contribute to shallowness of floor; assimilation of highland material into intruding magma may contribute to relatively high albedo of extrusions	2. Portions of floor embay wall scallops -- suggesting flowlike nature of floor unit; albedo of floor typically matches albedo of surrounding highlands
	3. Accumulation of light-colored ash on rim	3. Well-defined ejecta facies is absent but rim of crater is raised; profile due to remnant of crater-forming event (impact?) and/or volcanic material
	4. Slumping of wall enlarges crater slightly; structural modification involves most of floor because floor region corresponds more closely to size of intrusion	4. Perched ("hanging") craters on rim suggest crater enlargement; floor fractures typically extend to near floor-wall contact
B. Floor inundation	1. Emplacement of floor unit (light-colored flows or ash); narrow moat at floor edge due to flow termini or differential floor movement	1. Floor units extend into irregularities of crater plan; narrow moat marks contact at base of wall
	2. Magma reservoir enlarged but does not extend beyond crater boundary	2. Fractures outside crater generally absent; narrow moat marks contact at base of wall
C. Floor subsidence	1. Subsidence of inner floor block	1. Stereo imagery shows depressed floor interior, commonly surrounded by fractures
	2. Magma reservoir shrinks owing to withdrawal, crystalization, and/or volatile loss	2. Inferred from depressed inner floor; relatively quiescent subsidence inferred from absence of evidence for explosive phase
	3. Remnant of previous floor level remains on wall	3. Pronounced terrace-moat or ridge encircles floor; several examples exhibit inward-dipping floor plate parallel to wall or donutlike ring adjacent to wall
	4. Complex "plains" emplaced on portions or floor	4. "Plains" material form relatively well-defined contact with older hummocky floor material

Fig. 16. Unnamed Class IV A floor-fractured crater (−16°, 167°E) displaying narrow moat at floor edge with raised rim (A). Crater diameter is approximately 30 km. Solar illumination is from the left (west). Apollo 17 pan 1936.

that extends to the wall and embays wall scallops. A narrow moat (Figure 16, arrow A) separates the floor and wall owing to small differential floor movement or the termini of the flow. Evidence for lavalike emplacement includes the continuous nature of the narrow moat into wall scallops and adjacent overlapping craters. Numerous examples exhibit a low-relief lip along the floor edge (in a few examples well up on the wall) and a slightly depressed hummocky floor interior. This configuration could result from subsidence or sagging of the floor in response to volatile loss or shrinkage of the magma reservoir. Fractures at this stage typically form polygonal patterns restricted to the crater floor. Crater floors exhibiting narrow floor/wall moats but no floor fractures very possibly represent a related style of floor modification.

Further complexity of the floor results from subsidence of the inner floor block and this process is depicted in Figure 15c as floor collapse into the magma reservoir. A pronounced terrace-moat or ridge occurs along the floor edge in several Class IV craters (e.g., Bohnenberger), and owing to the continuity of the

ridge around large portions of the crater floor, it is interpreted as remnants of the previous floor level. In several examples, floor subsidence produces either an inward-dipping floor plate parallel to the wall or a doughnutlike ring adjacent to the wall. Complex 'plains' and mare units appear to have been emplaced subsequently on portions of the depressed floor within several craters. The 'plains' are hummocky in detail (0.3 km wavelengths) and typically have an albedo comparable to the more hummocky debrislike floor material and regions exterior to the crater. Extensive and complex (almost sinuous in a few cases) fracture patterns criss-cross the floor (see Figure 16). Well-defined radial fracture patterns occur in several examples and indicate either subsequent floor doming or subsidence of a floor unit over a stable buried mass.

Two other characteristics make Class IV floor-fractured craters unusual. First, their relatively small size should decrease the likelihood that they would tap a deeply seated lunar magma. Second, these craters commonly occur deep in the lunar highlands, a location that has been regarded as an unlikely site for lunar volcanism based on the Apollo 16 results. Perhaps these two phenomena indicate that this class of floor-fractured craters is related to the major basins. Moore *et al.* (1974) recognized depressions surrounding the Orientale Basin that contain fractured (fissured) floors and interpreted such units as impact melt. Such units are similar to those within Class IV A floor-fractured craters; however, generalization of this interpretation might not be warranted for the following reasons. First, the spatial distribution of such craters shows a highly asymmetric distribution with respect to the Orientale and Imbrium basins. Second, these craters do contain mare units, thereby implying related extrusions of basalts rather than deposition of impact ejecta. Third, Class IV craters commonly are very shallow. Large volumes of ballistic impact melt should not be retained within the crater after impact but should be dispersed as ejecta. Fourth, several examples show evidence for forming after the impact of a nearby well-preserved crater. For example, the floors of Class IV floor-fractured craters around Einstein A do not appear to have been modified by the formation of Einstein A, which overlies the Orientale ejecta blanket. Similarly, a pair of Class IV craters on the lunar farside (+16°, 174°E) exhibit floors apparently unmodified by the nearby impact Sharanov.

The devastating effects on the upper lunar crust from the formation of a major basin are difficult to assess owing to the large quantities of secondary and tertiary ejecta that were deposited. Theoretical estimates indicate that the shock and seismic effects were enormous (Schultz and Gault, 1975), and it is proposed that *some* floor-fractured craters (and particularly Class IV A craters north of the Orientale Basin) represent volcanic eruptions triggered by basin formation well before the stages of mare emplacement. The existence of dark mare units in these craters may indicate later volcanic rejuvenation along weaknesses and through vents originally related to basin formation.

B. RELATION TO THE MARIA

As noted above, the close spatial correlation between floor-fractured craters and the maria suggests a close genetic relation. In Figure 10, this relation was depicted as a link between a magma reservoir beneath a preexisting crater and a larger

magma chamber responsible for the maria. At least three models plausibly describe the location of the mare-producing magma chamber with respect to the modified craters. The first envisions the maria (or more precisely, the magma layer) extending beneath the highland borders at relatively shallow depths. This is the type of model that might be applicable for regional isostatic adjustment of pre-existing craters as suggested by Masursky (1964) and Daneš (1965). Daneš showed that appreciable isostatic compensation of a large crater theoretically results in a raised floor surrounded by a moat and a small depression concentric with the rim; Masursky recognized the similarity of this profile to Gassendi and similar craters. Such an explanation, however, does not account for the selectiveness of the process to certain craters of both widely different stages of degradation and different sizes. Masursky (1964) and Daneš (1965) did not specifically refer to such a model; rather, they depicted the adjustment as viscous flow of the upper lunar crust. It is possible that during the stages of mare flooding the upper highland crust exhibited a relatively low viscosity, but such a process still does not seem consistent with the variety in affected craters with respect to size and degree of preservation. Moreover, several large pre-mare craters exist that are encompassed by mare basalts, yet adjustment of the crater floor has not occurred. This preservation of crater profile suggests that any appreciable lowering of crustal viscosities also must have been local. Such selective phenomena seem more consistent with tapping a lunar magma chamber. Viscous flow and isostatic adjustment may be applicable, however, for certain heavily modified craters that extend into the maria (e.g., the craters in Mare Smythii) and for the older large basins such as Crisium and Humorum.

A second model involves pre-existing craters' tapping a magma layer that is directly related to the maria but occurs at greater depth than the preceding model. The fractured upper crust provides relatively easy passage for the fluid magma that collects beneath crater floors as depicted in Figure 10. Because many floor-fractured craters are concentrated along the mare shores, this model implicitly requires either the thinning of such a layer away from the maria or its greater depth.

Perhaps a more plausible model envisions pre-existing craters that indirectly tap a mare-related magma chamber by intersecting major dikes and sills at depth. Mason *et al.* (1975) have mapped major graben and ridge systems on the lunar farside and have found a strong radial and concentric pattern with respect to the Imbrium Basin. Such systems may have been initiated by the original basin impacts and may be important in later providing a link at depth between pre-existing craters and the maria. In particular, the concentration of floor-fractured craters in western Oceanus Procellarum might be related to intersecting crustal weaknesses from the Orientale and Imbrium Basins.

One of the last stages of volcanic activity within many floor-fractured craters is the emplacement of mare units. As noted above, relatively few of these craters contain mare units that have been fractured to the same degree as the other floor units. Moreover, few mare-filled craters exhibit floor fracturing. Consequently, there apparently has been little floor adjustment from volumetric changes of the magma reservoir due to parasitic eruptions, magma migration, volatile loss, or crystallization. In addition, significant changes in later eruptive products that reflect an evolved magma reservoir apparently did not occur.

There are three factors that contribute to this preservation of the high-level mare-flooding stage. First, modified mare-filled craters have not been properly identified. For example, the craters Lassell and Briggs A contain mare floors with a complex array of irregular depressions, thereby indicating floor adjustment by lava drainage rather than floor fracturing. More importantly, it was noted above that mare units within Gassendi show evidence of much higher levels with subsequent drainage. A similar sequence could be inferred from features and the albedo within Vitello. Consequently, the floors of some floor-fractured craters may have undergone complete inundation with subsequent withdrawal and further floor fracturing, and the resulting floor morphology no longer resembles a mare-filled crater.

A second contribution to the absence of fractured mare craters is the type of eruption responsible for the inundation of the maria. Greeley (1975) has suggested that the early stages (Imbrian) of mare flooding were comparable to the massive flood basalts on Earth, whereas the later (Eratosthenian) eruptions were of lesser volume and over extended periods of time. Relatively catastrophic volcanism represented by the emplacement of flood basalts must have interrupted – and, in some regions, culminated – longer term volcanic processes. During the early stages of lunar volcanism, pre-existing and newly formed impact craters probably were sites of volcanic modification spatially remote from surface flows just as floor-fractured craters now occur several hundred kilometers from the mare shore. As these massive eruptions affected greater areas, previously volcanically modified craters closest to the source would become primary vents. Previous stages of floor volcanism reflecting processes such as the geochemical evolution of the magma reservoir and the assimilation of local crustal materials would be supplanted by the conditions of the primary magma chamber responsible for the flood basalts. Thus the observation that many floor-fractured craters near the maria contain mare units as their last eruptive phase is no more significant than the observation that the maria do not exhibit features departing significantly from those characteristic of fluid basaltic eruptions.

A third explanation for the absence of fracturing in mare-filled craters follows the suggestion that some floor-fractured craters represent sites of volcanism generated by a major basin impact. In particular, there may have been two completely unrelated stages of volcanism, the last being the stage of mare flooding.

The crater Alphonsus may provide an example of pre-basin floor modification. Specifically, it exhibits a modest central peak approximately 1.2 km above the floor, which is clearly modified by Imbrium-related ejecta, whereas the peak-rim elevation difference is between 0.6 km (western rim) and 1.2 km (eastern rim), values that are comparable to extensively modified floor-fractured craters. However, Alphonsus does not exhibit extensive floor modification, and it is possible that floor uplift in Alphonsus predated the Imbrium impact.

C. TYPE OF INTRUSION

Except for the most extensively modified craters, modification is restricted to the crater interior. If the intruding igneous magma was deeply seated relative to the crater diameter, then the resulting modification should extend beyond the crater rim as either radial fractures or cone sheets. The response of the crater floor to

the intrusion may provide some clues to its type and depth. In their discussion of terrestrial resurgent cauldrons, Smith and Bailey (1968) point out that small thickness to diameter ratios (<0.25) of the resurgent block make the block more prone to doming by upward-directed magma pressure. The majority of lunar floor-fractured craters, however, do not exhibit strong radial floor fractures. This observation may reflect the fact that we now observe only the end result of modification. It also might indicate a thickness-diameter ratio between 0.5 and 1.0. For a 40 km diameter crater, this suggests a depth between 15 km and 30 km because the floor diameter would be approximately 30 km. For an impact crater of the same size, the transient crater depth was probably between 7 km and 10 km, whereas the zone of extensive shattering and fracturing may extend down to approximately 0.5 to 1.0 the crater diameter. This would be consistent with the hypothesis that the magma is collected in a reservoir beneath the crater.

If the intrusion is a relatively dense mafic magma, then two questions arise. First, what was the driving force for floor elevation? Second, how would a fluid magma intrude? Figure 6 indicates that in general the elevation of the floor approximates that of the surrounding mare units. Consequently, magmastatic adjustment is thought to be a likely driving force in numerous instances. This adjustment is isostatic in that an equilibrium level is sought, but it is not isostatic in the same regional sense as implied by Masursky (1964) and Daneš (1965). The restriction of the adjustment to the crater floor, the evidence for floor volcanism, and the selectivity of certain craters for modification favor the interpretation that the crater floor has become a conduit directly or indirectly connected to the mare magma chamber. Because the central peak complex and old wall material typically have been raised, the old floor is pictured as floating on an intruded reservoir (sill) of marelike material. This buoyant force is in contrast to the deeply seated upward force produced by viscous silicic intrusions in terrestrial resurgent cauldrons. In further contrast, the fluid magma generally will follow pre-existing weaknesses. Regional elevation of the mare level with time might reflect an enlarging magma chamber or perhaps ancient tides generated by much closer approaches to the Earth during the epochs of mare emplacement (Schultz, 1972; Sjogren and Wollenhaupt, 1975).

Extending the hypothesis of magmastatic adjustment, one can obtain either a very approximate value of the density difference between the magma and floor block, where the thickness of the block is assumed, or an approximation of the thickness of the floor block where a density difference is assumed. If the height (h) of the floor above the surrounding mare level reflects only the height of the exposed buoyed mass, then the total thickness (t) of the block is expressed simply by

$$t = \frac{h\rho}{\Delta\rho},$$

where ρ is the density of the intrusion and $\Delta\rho$ is the density difference between the intrusion and the floor block. Figure 17 illustrates these dependencies. For given values of floor height, smaller density differences indicate thicker floor blocks. Figure 6 shows that 30 km diameter craters in Mare Smythii typically exhibit floor heights of 0.2 km above the mare plains. Consequently, for $\Delta\rho = 0.1$, the block

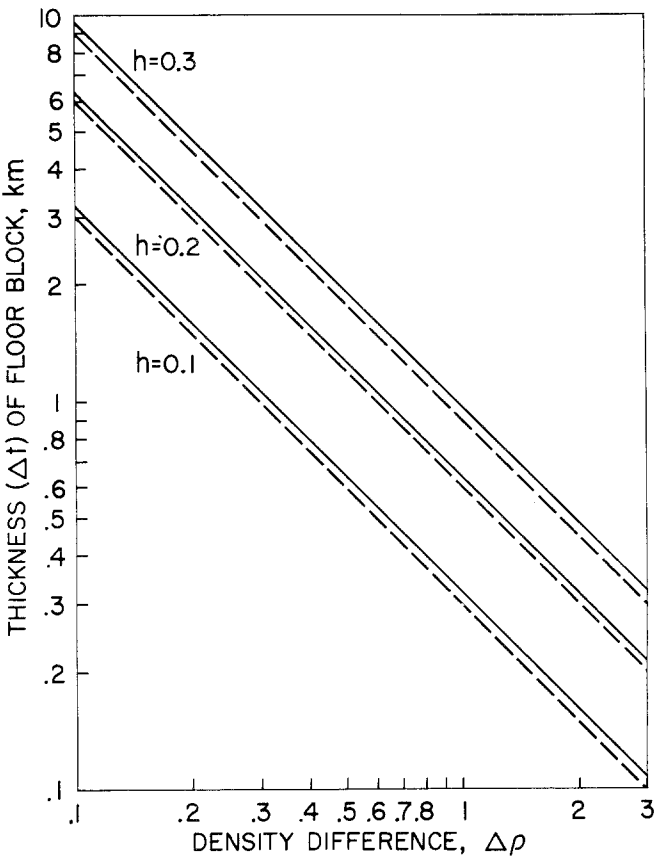

Fig. 17. Thickness of buoyed floor block (Δt) as determined by the elevation of the floor above the local mare level (h, in km) and the difference in density ($\Delta\rho$) between the floor block and the intruding magma. Solid lines correspond to an assumed density of 3.2 g/cm^3 for intruding magma; dashed lines, to a density of 3.0 g/cm^3.

thickness is approximately 6 km. If the transient crater diameter was 20 km, then the ratio of this depth to the transient diameter is 1 : 3.7. Note that the assumed density of the intruding mass has little effect on this result. Conversely, if the thickness of the block corresponds to the horizon of extensive shock-induced brecciation below a 20 km diameter (D) impact crater, then for $t : D$ given by 1 : 3, the density difference is 0.095.

It was noted above that blocklike uplift generally implies a ratio of block thickness to block diameter of 1 : 4 to 1 : 1. Smaller ratios tend to produce floor doming and radial tension fractures. A sill-type intrusion and welded floor cap would tend to reduce the ratio owing to a more uniformly applied upward stress and a relatively uniform response to this stress, a situation that is consistent with the implications from Figure 17. Conversely, the blocklike floor uplift with thickness-diameter ratios greater than 0.3 suggests a very small difference in density between the intruding mass and the floor block. Such a small difference could be partly due to both

extensive filling of interstitial fractures in the floor block by the intruding magma and emplacement of volcanic units on the crater floor.

A small density difference between the intruding mass and old crater floor suggests that floor-fractured craters should not produce strong gravity anomalies. Gravimetric data (Sjogren *et al.*, 1972; Sjogren and Wollenhaupt, 1973) for the craters Gassendi, Doppelmayer, Vitello, Alphonsus, Arzachel, Ritter, Sabine, and Hevelius do not show pronounced positive or negative signatures and generally blend with the regional trend of gravity contours. A possibly important exception is the crater Taruntius, which is spatially associated with a strong (+50 mgal) elongate anomaly as indicated in the Apollo 16 subsatellite data of Sjogren *et al.* (1974). Two factors besides the density of the crater fill material will influence the gravimetric data. First, the spatial resolution of the processed Apollo subsatellite data will mask small gravity anomalies associated with craters less than 100 km in diameter. Second, a deep-seated intrusion such as a sill at depth will not be as readily detectable as an equivalent extrusive mass. For illustration, a plate of density 3.5, thickness 2.2 km, and radius 30 km will produce a positive gravity anomaly of 42 mgals as recorded by a satellite at an altitude of 26 km (from computer-generated simulations supplied by W. L. Sjogren). Burial of this mass at a depth of 59 km (0.6D for Copernicus) produces a positive anomaly of only 10 mgals. These simulations and the gravity data suggest that a large intrusive plug of dense mantle material beneath the sampled floor-fractured craters (with the exception of Taruntius) is unlikely, but the data are consistent with a sill-type reservoir situated between 0.5D and 0.8D beneath the crater floor where D is the crater diameter.

The enigmatic absence of a gravity anomaly associated with Sinus Iridum (Muller and Sjogren, 1968) is thought to be related to its development as a floor-fractured crater. The present mare fill is believed to cap an elevated floor block beneath which is a sill-type intrusion having relatively minor density difference. Thus in the case of Sinus Iridum, the floor neither foundered nor filled with dense basalts, as might be inferred from its appearance. Nor did the Iridum impact immediately tap and fill with basalts associated with Imbrium. The ghost ring Lamont, however, is interpreted as a heavily modified impact crater. Its strong positive gravity anomaly is an expression of both floor foundering and the development of an enlarged resevoir or plug, thereby effectively transforming an impact crater into a caldera. The floor-fractured crater Taruntius and the mare-filled crater Crüger exhibit pronounced positive anomalies and are interpreted as exposed analogs of Lamont.

5. Summarizing Remarks

The preceding results and discussions indicate that floor-fractured craters have significance for the style of crater modification, the type of lunar volcanism, the sequence of inundation of the maria, and the thermal history of the Moon. These points are summarized below.

A. CRATER MODIFICATION

The statistical data and morphology of floor-fractured craters indicate that impact craters have become the centers of intrusions and volcanism generally related to the periods of inundation of the basins by mare basalts. Such modification ranges from

extensive fracturing and uplift of crater floors (Gassendi) to more subtle debris-laden floors (Krieger). During the early stages of modification, volcanism is contained within the crater. As modification progresses, the old crater floor and central peak complex passively rise. The most extensive modification results in capping the elevated crater floor with mare basalts and eruptions in the crater rim region.

The sequence of modification developed from this study accounts for the following features:

(1) Exposures of central peaks within mare-filled craters
(2) The enigmatic negative gravity anomaly associated with mare-flooded craters
(3) The association of sinuous rilles and crater rims of mare-flooded craters
(4) Modification of craters of widely differing sizes and ages
(5) Multi-ringed plan of craters such as Gassendi and Posidonius
(6) The ridgelike and platformlike rim profiles of ringed plains in the maria

In addition, there is evidence that certain craters were inundated by mare basalts either without significant floor elevation or with subsequent foundering of the old floor owing to the weight of repeated extrusions of mare basalts. The latter sequence is associated with thick surface and subsurface accumulations of basalts that should contribute to strong positive gravity anomalies – e.g., Crüger, Grimaldi, or Lamont.

Although mare-filled craters typically do not exhibit subsequent structural modification, this observation is probably in part the result of an implicit assumption that the present degree of mare inundation represents the maximum extent of inundation. It is proposed that some of the fractured plains within Class II and III craters represent surfaces once inundated by mare basalts that subsequently drained back into vents.

B. TYPE OF LUNAR VOLCANISM

As volcanic vent structures, the fractured floors of large modified impact craters present possible evidence for a new variety of lunar volcanism. Because these vents apparently were linked to the magma chamber or mantle layer responsible for the mare plains, they exhibit, in general, eruptive products similar to those around the maria. In addition, however, eruptions of relatively high albedo material probably occurred, perhaps as a result of (1) assimilation of highland-type crustal material into a marelike magma reservoir and/or (2) a separate eruptive phase triggered by a basin-forming impact. Either alternative raises the possibility that some light plains units in the highlands are due not only to impact ejecta but also to extrusions of light-colored lava or ash. Not all floor-fractured craters are closely associated with the large maria, and these exceptions may hold important clues to the type, extent, and time of highland volcanism.

C. INUNDATION OF THE MARIA

The inferred link between the maria and floor-fractured craters suggests that such craters may become important volcanic vents that contribute to the inundation of the lunar surface by mare basalts. Mare Australe illustrates a mare region in which most of the mare units are contained within craters. From this study, it is believed that these mare-filled craters had undergone a stage of floor fracturing prior to

inundation. Ringed plains indicate not only inundation but also extensive structural modification of the crater floor and rim. If the concentration of floor-fractured craters west of Oceanus Procellarum represents a precursory stage of mare flooding, then numerous buried vents can be inferred in this and other irregular maria.

D. INTERNAL THERMAL HISTORY

Floor-fractured craters might be a useful diagnostic tool for the identification of internal processes where other clues are absent or ambiguous. Their occurrence in the lunar highlands suggests that these regions did not fully escape the epochs of mare flooding. Similarly, their occurrence along the borders of the plains regions on Mars suggest internal processes analogous to the mare plains (Schultz *et al.*, 1973).

Further studies of floor-fractured craters should provide insight for the inundation sequence of the maria, in their roles both as parasitic and primary eruptive centers and as models for inundation of the much larger mare-filled basins.

Acknowledgements

I gratefully acknowledge the constructive reviews by R. Greeley, J. Guest, D. Gault, and D. Wilhelms. In addition, W. Sjogren provided computer simulations of the gravimetric data and his generosity is greatly appreciated. This research was performed while the author was a National Research Council – National Academy of Science Resident Research Associate at NASA Ames Research Center.

References

Baldwin, R. B.: 1963, *The Measure of the Moon*, University of Chicago Press. 488p

Brennan, W. J.: 1975, 'Modification of Premare Impact Craters by Volcanism and Tectonism', *The Moon* **12**, 449–461.

Cameron, W. S. and Padgett, J. L.: 1974, 'Possible Lunar Ring Dikes', *The Moon* **9**, 249–294.

Daneš, Z. F.: 1965, 'Rebound Processes in Large Craters', In *Astrogeologic Studies*, pp. 81–100, U.S. Geol. Survey open file ann. prog. rept., pt. A.

De Hon, R.: 1971, 'Cauldron Subsidence in Lunar Craters Ritter and Sabine', *J. Geophys. Res.* **76**, 5712–5718.

Dence, M. R.: 1971, 'Impact Melts', *J. Geophys Res.* **76**, 5552–5565.

Gault, D. E., Quaide, W. L., and Oberbeck, V. R.: 1968, 'Impact Cratering Mechanics and Structures', In *Shock Metamorphism of Natural Materials*, p. 87–99. B. French and N. Short (eds). Mono Book Corp., Baltimore. 644p.

Greely, R.: 1975, 'A Model for the Emplacement of Lunar Basin-Filling Basalts', *Lunar Science* **VI**, 309–310. Lunar Science Institute, Houston.

Mason, R., Guest, J. E., and Cooke, G. N.: 1975, 'An Imbrium Pattern of Grabens on the Moon', *Proc. Geol. Assoc.* (in press).

Masursky, H.: 1964, 'A Preliminary Report on the Role of Isostastic Rebound in the Geologic Development of Lunar Crater Ptolemaeus', In *Astrogeologic Studies*, pp. 103–134, U.S. Geol. Survey open file ann. prog. rept., pt A.

Moore, H. J., Hodges, C. A., and Scott, D. H.: 1974, 'Multiringed Basins – Illustrated by Orientale and Associated Features', In *Proc. Fifth Lunar Sci. Conf., Geochem. Cosmochim. Acta*, Suppl. 5, Vol. 1, pp. 71–100. Pergamon.

Muller, P. M. and Sjogren, W. L.: 1968, 'Mascons: Lunar Mass Concentrations', *Science* **161**, 680–684.

Quaide, W. L., Gault, D. E., and Schmidt, R. A.: 1965, 'Gravitative Effects on Lunar Impact Structures', In *Geological Problems in Lunar Research*, pp. 563–572, Annals N.Y. Acad. Sci. **123**.

Pike, R. J.: 1968, 'Meteoritic Origin and Consequent Endogenic Modification of Large Lunar Craters – A Study in Analytical Geomorphology', Ph. D. thesis, University of Michigan, 404p.
Schultz, P. H.: 1972, 'A Preliminary Morphologic Study of Lunar Surface Features', Ph.D. thesis, University of Texas at Austin, 967p.
Schultz, P. H.: 1974, 'Floor-fractured Lunar Craters', *Lunar Science* V, 681–683. Lunar Science Institute, Houston.
Schultz, P. H.: 1976, *Moon Morphology*, University of Texas Press, Austin.
Schultz, P. H. and Gault, D. E.: 1975, 'Seismic Effects from Major Basin Formation on the Moon and Mercury', *The Moon*, **12**, 159–177.
Schultz, P. H., Manley, W. D., Jr., and Ingerson, F. E.: 1973, 'Comparison of Lunar and Martian Crater Floors (abs.)', *Trans. Amer. Geophys. Union* **54**, 1127.
Sjogren, W. L. and Wollenhaupt, W. R.: 1973, 'Gravity: Mare Humorum', *The Moon* **8**, 25–32.
Sjogren, W. L. and Wollenhaupt, W. R.: 1975, 'Lunar Maria Figure', *Lunar Science* VI, Lunar Science Institute, Houston.
Sjogren, W. L., Muller, P. M., and Wollenhaupt, W. R.: 1972, 'S-Band Transponder Experiment', In *Apollo 16 Preliminary Science Report*, pp. 24 : 1–24 : 7. NASA SP–315.
Sjogren, W. L., Wimberly, R. W., and Wollenhaupt, W. R.: 1974, 'Lunar Gravity via the Apollo 15 and 16 Subsatellites', *The Moon*, **9**, 115–128.
Smith, R. L. and Bailey, R. A.: 1968, 'Resurgent Cauldrons', In R. R. Coats, R. L. Hay, and C. A. Anderson (eds.), *Studies in Volcanology*, pp. 613–662, Geol. Soc. Amer. Mem. 116.
Whitford-Stark, J. L.: 1974, 'Internal Origin for Lunar Rilled Craters and the Maria?', *Nature*, **248**, 573–575.
Wood, C. A.: 1974, 'External Origin for Lunar Rilled Craters and Mare Basins', *Nature* **251**, 166.
Young, R. A.: 1972, 'Lunar Volcanism: Fracture Patterns and Rilles in Marginal Premare Craters', In *Apollo 16 Preliminary Science Report*, pp. 29 : 89–29 : 90. NASA SP–315.